Planar microwave resonator with electrodeposited ZnO thin film for ultraviolet detection

M. Benlamri,[1] S. Deif,[1] N. Mahdi,[1] M. Baghelani,[1,2] M. H. Zarifi,[3] D.W. Barlage,[1] K. Shankar,[1,4] and M. Daneshmand[1]

[1]Department of Electrical and Computer Engineering, University of Alberta, Edmonton, Alberta, T6G 2V4, Canada
[2] Department of Electrical Engineering, Ilam University, Ilam, Iran
[3]Department of Electrical Engineering, University of British Columbia, Kelowna, BC, V1V 1V7, Canada
[4]National Institute for Nanotechnology, National Research Council, Edmonton, Alberta, T6G 2M9, Canada

E-mail: daneshmand@ualberta.ca

Received xxxxxx
Accepted for publication xxxxxx
Published xxxxxx

Abstract

A ZnO thin film is electrodeposited on the conducting strips of a planar microwave ring resonator to enable the formation of a novel sensor for ultraviolet irradiation. The fabrication of the sensor involves a low-cost process that basically utilizes a printed circuit board and an aqueous precursor solution. The resonator with no ZnO coating operates with a resonant frequency of 6.2 GHz and a quality factor of 170. The time-resolved microwave photoresponse of the sensor to UV illumination, under ambient conditions, is assessed through measurements of the resonance profile of the S_{21} parameter. The resonance frequency exhibited a highly sensitive downshift of ~ 6 MHz after a UV illumination time of ~ 3 min. This downshift is mostly attributed to the change in the dielectric constant of the ZnO film caused largely by the additional creation of bound charges. The usually reported long-lived and persistent post-illumination effects were not observed. The measurements of the resonance amplitude carried out at 20% and 70% relative humidities revealed average excess carrier relaxation lifetimes of 213 s and 185 s, respectively. Concomitantly, the measured resonance frequency downshift increased with increased humidity. These results highlight the difference in the interaction mechanisms of photogenerated carriers with water and oxygen molecules on the surface and grain boundaries of the ZnO film. To our knowledge, this UV irradiation sensor is the first ZnO-based sensor device implemented with planar microwave circuit technology. In addition, the capabilities demonstrated by this simple photosensing method to determine induced carrier lifetimes make it a valuable technique for in-depth investigation of the material properties.

Keywords: dielectric constant, planar microwave sensor, microstrip resonator, ultraviolet sensor, photosensor, zinc oxide, electrodeposition, carrier dynamics.

---

1. Introduction

Zinc oxide (ZnO) is a wide bandgap metal oxide semiconductor (E_g = 3.37 eV) with a large exciton binding energy at room temperature (E_b = 60 meV), a high maximum electron mobility at room temperature (~ 200 $cm^2 V^{-1} s^{-1}$), a high electron saturation velocity (> 3×10^7 $cm\ s^{-1}$), and a high maximum breakdown field [1-4]. The combination of these properties coupled with their earth abundance and solution processability render ZnO thin films and nanostructures attractive material platforms for a range of optoelectronic devices including, but not limited to, ultraviolet photodetectors [5, 6], ultraviolet light emitting diodes [7, 8], gas sensors [9], electron transport layers in low-cost solar cells [10], thin film transistors [11, 12], and power electronic devices [13, 14]. At the same time, ZnO thin films and nanostructures exhibit a large dispersion in their electronic

parameters depending on factors such as film morphology, stoichiometry, crystallinity, surface-bound species, and quality of hetero-interfaces in devices containing heterojunctions. Therefore, improved methods to characterize the optoelectronic properties of ZnO and other metal oxide semiconductors remain an enduring area of research and development.

Microwave resonators and sensors are well-studied and used in communication systems [15-20]. However, the microwave resonators with the planar configuration have recently gained a lot of interest for sensing applications due to their simplicity, low cost, low profile, long lifetime, non-contact sensing capability, and their compatibility with CMOS technology which facilitates mass production. These sensors can be used for material characterization [21-25], gas and liquid detection [26-28], and also for biomedical diagnostic applications [29-31]. In addition, microwave sensors, in general, do not require special sample preparation.

In this regard, our group recently reported on the use of planar microwave resonators to measure the time-resolved microwave conductivity (TRMC) in bare and surface functionalized TiO_2 nanotube arrays [24, 32, 33]. For TRMC measurements, planar microwave resonators possess distinct advantages over cavity waveguide resonators such as CMOS integrability, compactness, clearly defined regions of maximum microwave amplitude, and high sensitivity to both photodielectric and photoconductive effects [32]. TRMC measurement in ring-type planar microwave resonators involves placing a free-standing membrane or film grown on a non-conductive substrate, of the material to be measured, in the coupling gap of the resonator where the microwave field is strongest. For thin films that cannot be delaminated from their underlying substrate, and also when the films can only be grown on conductive substrates as in electrodeposited films, an alternative measurement configuration is needed to capture the characterization benefits of planar microwave resonators. Keeping this in mind, we report on planar microwave resonators where the ZnO film to be characterized is directly electrodeposited on the conducting copper (Cu) strip lines forming the resonator on a printed circuit board (PCB). Indeed, during electrodeposition, the ZnO film is deposited exclusively on the conducting copper strip lines and not on the nonconducting areas on the circuit board. The great advantage of this direct and selective electrodeposition on the conducting strip line is that no photolithographic processing or other resource-intensive patterning methods are needed, beyond the basic PCB circuit layout, to form the deposition pattern, thereby greatly simplifying the overall fabrication process. This process optimization explains our choice of PCB-mounted planar microwave resonators for photoresponse characterization through TRMC measurement. More traditional methods of photodetection are based on employing devices such as metal-semiconductor-metal photodetectors and measuring the photocurrent between the metal contacts at fixed bias voltage. By using the contactless TRMC method, a further process simplification is gained by eliminating the metal contacts deposition step. The TRMC method is based on the measurement of changes in microwave power with time when the sample is subjected to a short illumination [34]. Photogenerated charges in the semiconductor film can modify both the real and the imaginary parts of its permittivity depending on their mobility and degree of localization [35]. The film complex conductivity σ relates to its complex permittivity $\varepsilon = \varepsilon' - i\varepsilon''$ as:

$$\sigma = i\omega\varepsilon = \varepsilon_0\omega\,(i\varepsilon' + \varepsilon'') \tag{1}$$

where ω is the angular frequency of a microwave electric field, ε_0 is the vacuum permittivity, and ε' and ε'' are the real and imaginary parts of the permittivity respectively. Therefore, the imaginary part of the permittivity identifies microwave absorption whereas the real part is associated with polarization and is responsible for a shift in the resonance frequency of the electric field. Both the real and imaginary parts of the electrical permittivity (and hence the complex conductivity) of the deposited film can be extracted by measuring two of the following characteristics of the microwave signal: amplitude, frequency, and quality factor [32]. These characteristics are readily extractable from the S-parameters of the microwave resonator. For photoresponse measurements, we monitor the variations in resonance frequency f_r, resonance amplitude A_r, and quality factor Q in response to ultra-violet (UV) illumination as a function of time.

TRMC offers other advantages over alternative techniques as well. In the case of direct current (DC) photoconductivity, the measurements suffer from charge transfer distortions at the metal-semiconductor interfaces through recombination, trapping, and back-injection. Another advantage is the capabity of the TRMC method to explore the carrier dynamics and determine the carrier relaxation lifetimes and the excess carrier decay mechanisms. In general, different optoelectronic properties can be exploited to realize carrier lifetime measurements, the most common being photoluminescence (measures radiative decay of

excess carriers), photoconductance (captures the behavior of mobile carrier), and photovoltaic response (requires an internal driving force for charge separation). Many measurement techniques based on these concepts have been developed. On the other hand, TRMC is able to provide insight into the behavior of both mobile and immobile (trapped) carriers without any constraint on whether they relax radiatively or non-radiatively. TRMC has been used to characterize semiconductors such as silicon [36] and titanium oxide (TiO_2) [32] but no substantial TRMC studies have been reported on ZnO. The lifetime results available in the literature pertain to photodetector structures with electrodes show variation from few microseconds [37] to hours depending on the film structure, growth condition, and measurement techniques, thereby some exhibiting the persistent photoconductivity (PPC) behavior [38].

Electrodeposited ZnO films of high stoichiometric and crystalline quality have recently been synthesized by our group on copper and platinum (Pt), and demonstrated to result in Schottky diodes with superior transport and ideality factors [39, 40], as compared to films prepared by conventional ZnO solution processing techniques [41].

ZnO shows a tendency to exhibit strong PPC when illuminated by both supra-bandgap and sub-bandgap photons. There is strong fundamental interest in understanding the photoconductivity and PPC phenomena in ZnO due to 1) a range of interesting effects such as adsorption of O_2 and emission of CO_2 akin to the lungs of living creatures [42], the need for methods to control the PPC and resulting charge storage, and 2) the highly contested mechanism responsible for the PPC [43]. The PPC phenomenon enables ZnO-based thin films and nanostructures to be considered for charge storage applications but is undesirable in photodetectors due to the lengthening of response and relaxation times [44, 45].

In this work, a novel technique using planar microwave ring resonators coated with electrodeposited ZnO thin films is implemented to fabricate microwave sensors with detection capabilities to UV light irradiation. The UV detection sensitivity of the ZnO thin film is assessed through analysis of the S-parameters of the resonator sensor in the microwave frequency region. The effect of ambient humidity change on these photoresponse measurements is also experimentally examined.

2. Experimental

2.1 Methodology

A planar microwave ring resonator is designed and simulated in HFSS software. The transmission parameter S_{21} is studied for various dielectric conditions (permittivity and conductivity) of a thin semiconducting layer of electrodeposited ZnO that conformally coats the top microstrip lines. The intimate contact of the ZnO layer with microstrip copper lines forms a Schottky contact with a space charge region at equilibrium, the width of which depends on the carrier concentration in ZnO, the relative permittivity, and the built-in potential. The ring microstrip resonator structure is presented in figure 1(a). The resonator is capacitively coupled to input and output microstrip lines. The microwave signal is injected from port 1, while port 2 is terminated to ground with a 50 Ω load during the simulation of the transmission parameter S_{21}.

The simulation results of the S_{21} resonance profile of the bare (no ZnO film) microstrip resonator are presented in figure 1(b). They demonstrate a resonance frequency of 6.2 GHz and a quality factor of 170 with a resonance amplitude of -8 dB. Electric field analysis at the resonance frequency demonstrates the intense electric field on the resonator's microstrip gap, while the magnetic current simulation distribution presents the intensity of the magnetic current in specific regions of the resonator's microstrip line (figures 1(c) and 1(d)).

The introduction of the semiconducting ZnO layer in the immediate vicinity of the microwave resonator alters the electromagnetic fields in that region and therefore results in the variation of the effective permittivity representing the combined permittivity values associated with all the materials forming the resonator sensor multi-media system. Moreover, as discussed previously, the TRMC method is based on the temporal variations of the resonator's complex permittivity (and therefore complex conductivity). Indeed, the microwave resonator's photoresponse is a measure of the variation of the complex permittivity as a function of time when subjected to a short UV illumination. As will be discussed later, the variations of the complex permittivity are physically caused by multiple photogenerated carrier processes. Thus, to represent the permittivity variations due to UV illumination for simulation purposes, we assign hypothetical values and changes to the permittivity $\varepsilon = \varepsilon' - i\varepsilon''$ through the traditionally employed input parameters: dielectric constant $\varepsilon_r = \varepsilon'/\varepsilon_0$ and loss tangent (tan δ).

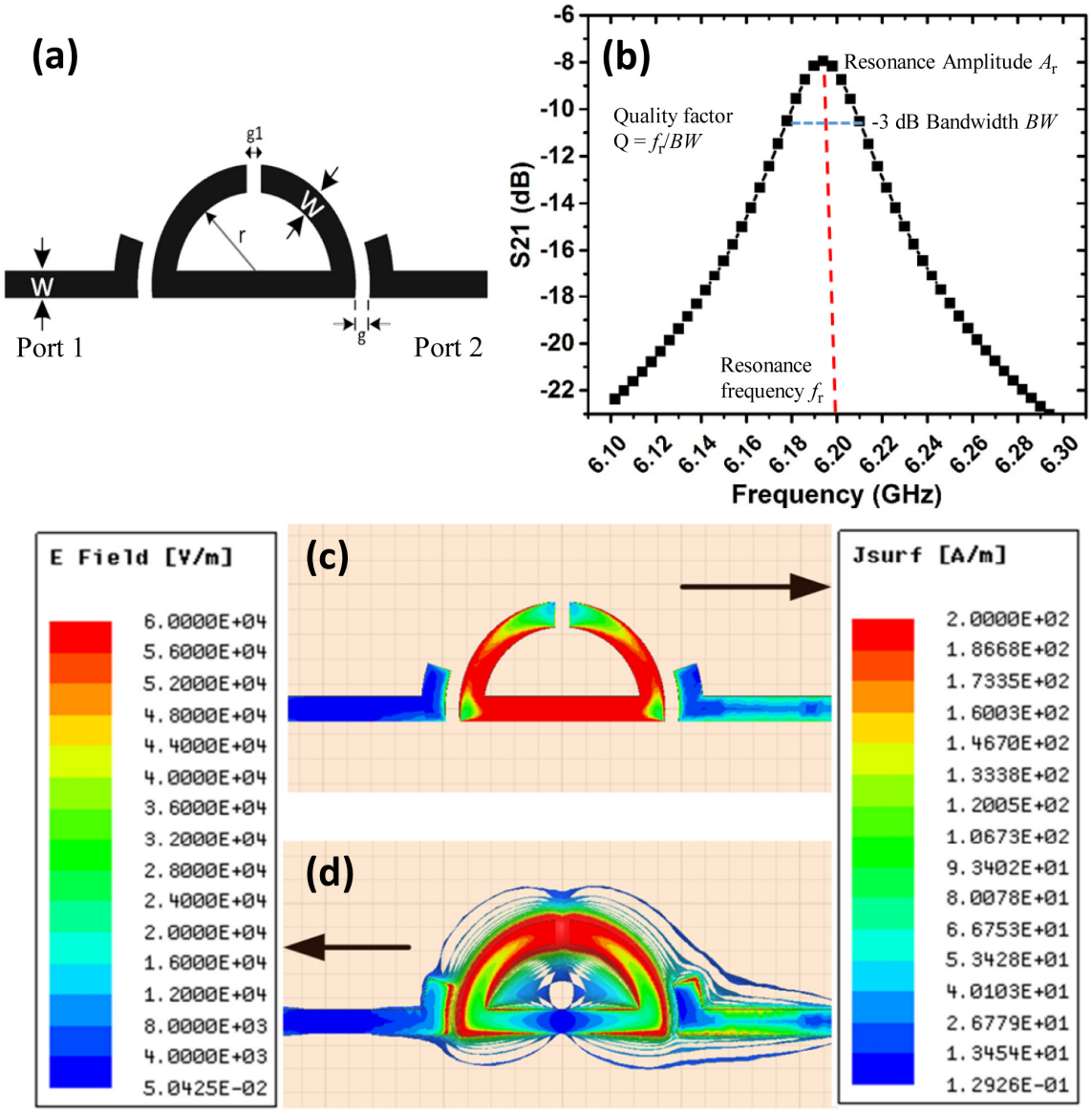

Figure 1. (a) Curved ring resonator implemented in HFSS, W = 1 mm, g = 0.6 mm, g_1 = 0.6 mm, r = 2.8 mm, (b) simulated S_{21} resonance profile with resonance frequency and quality factor of 6.2 GHz and 170, respectively, (c) magnetic current distribution on the resonator's microstrip lines, and (d) electric field simulation on the resonator's substrate.

To study the effect of the ZnO thin film electrodeposition on the electrical parameters of the resonator, a model was implemented in HFSS and simulated using the finite element method. Figure 2 presents the implemented structure and the simulation results for the S_{21} resonance profile for varying electrical parameters (dielectric constant, loss tangent) of the ZnO thin layer. The dielectric constant of the ZnO thin film was assumed to be 8.9 [46]. Firstly, figure 2(a) demonstrates that both the resonance frequency and the resonance amplitude are significantly affected by the presence of the electrodeposited ZnO film. The ZnO film creates excess regions of higher dielectric constants and finite conductivities in the immediate vicinity of the resonator, which result in these changes of the transmitted microwave energy. It should be noted that the ZnO electrodeposition effect on the microstrip's gap capacitance should be relatively weak. Secondly, the simulation in figure 2(b)

shows the S_{21} results for varying input values of the dielectric constant and tangent loss of a ZnO layer of 4.7 µm thickness. The corresponding resonance frequencies f_r and resonance amplitudes A_r are given in table 1.

Table 1. Resonance frequencies f_r and resonance amplitudes A_r which correspond to the S_{21} simulation plots of figure 2(b).

ε_r	tan δ	f_r (GHz)	A_r (dB)
8.9	0.01	6.169400	-7.517
11	0.01	6.168790	-7.525
11	0.5	6.168670	-9.674

It is observed that an increase of ε_r from 8.9 to 11 with a constant tan δ of 0.01 leads mainly to a frequency downshift. On the other hand, an increase of tan δ from 0.01 to 0.5 with a constant ε_r of 11 leads mainly to an amplitude decrease with relatively minor frequeny variation. The space charge region at the copper/ZnO interface has not been considered in this simulation. The observed resonance frequency downshift can therefore be mostly attributed to the variations of the resonator's effective dielectric constant. The capability of this experimental method to selectively detect the variations to the probing microwave signal caused by changes in the resonator's dielectric environment leads us therefore to conclude that such method could be effectively used to characterize the electrical properties of the ZnO thin film.

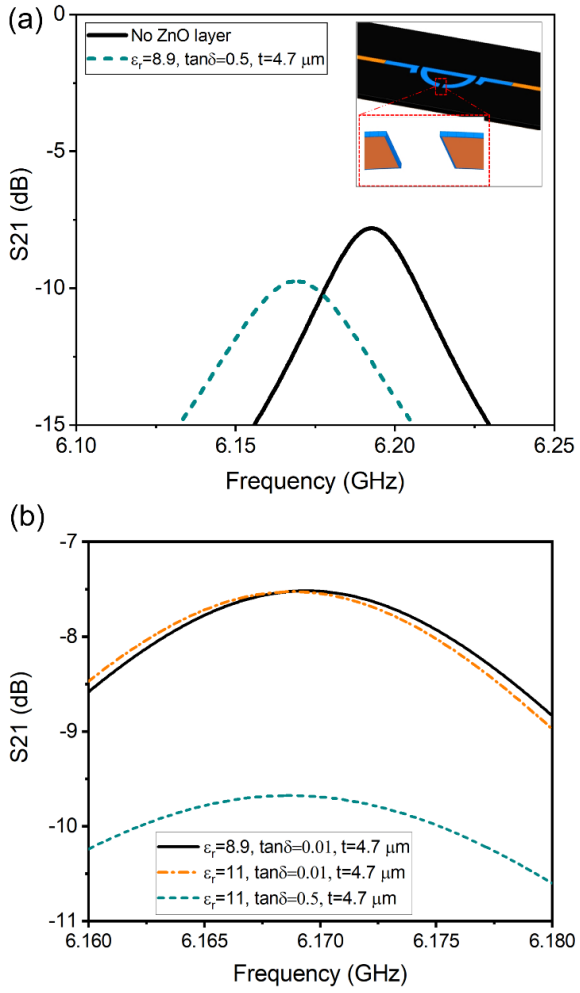

Figure 2. (a) Simulation results show the frequency downshift after ZnO film electrodeposition. The inset illustrates the

simulated structure in HFSS software with a layer representing ZnO (blue color) on the copper microstrips (orange color). (b) the simulation results for varying values of the dielectric constant and tangent loss of a ZnO layer of 4.7 μm thickness.

2.2 Fabrication

The growth of the ZnO thin film by electrodeposition presents significant advantages. Firstly, electrodeposition is a low-cost and simple solution technique with potential to grow high quality ZnO films at low temperatures. Secondly, the fabricated resonator copper structure readily forms a selective conductive pattern for ZnO electrodeposition. No complex photolithographical pattern alignment steps are therefore needed between the copper understructure and the ZnO film coating it. This seamless and simple fabrication process is achievable with minimal time and costs.

The planar microwave resonator sensor, shown in figure 3(a), was implemented on a microwave substrate, from Rogers Corporation, with the following specifications: dielectric constant = 2.2, loss factor = 0.00009, thickness of the dielectric material = 0.79 mm, and thickness of copper layer (covering both sides of the substrate) = 35 μm. A PCB processing technique using wet chemical etching was applied to implement the microwave resonator.

Cathodic electrodeposition was employed to grow thick ZnO films on the fabricated resonator's copper strips. The electrolytic solution consisted of 100 mM zinc nitrate hexahydrate (99%, Sigma-Aldrich) dissolved in deionized water. The initial solution pH was 5.2 ± 0.2. The deposition mechanism of ZnO film from the zinc nitrate $Zn(NO_3)_2$ precursor in aqueous solution has been described in detail in a previous work [39]. Prior to ZnO electrodeposition, the rough surface of the fabricated resonator copper structure was rinsed in acetone and methanol and subjected to a soft oxygen plasma treatment of 10 s duration. The purpose of this treatment is to achieve good adhesion at the copper/ZnO interface through contamination removal and surface activation. The electrodeposition process was carried out potentiostatically using a standard three-electrode cell configuration in a glass beaker. The reference electrode was a standard Ag/AgCl electrode (+200 mV vs SHE, the standard hydrogen electrode). A sputtered platinum film and the pretreated resonator copper structure were set up as counter electrode and working electrode respectively. Electrodeposition cannot be performed on the as-fabricated resonator copper structure because the two feed lines and ring are spatially separated by the two coupling gaps which do not allow current flow to all parts of the copper structure. To this effect, two connecting thin wires were placed by soldering between each feed line and the ring respectively. A computer-controlled CHI660E electrochemical workstation was employed to apply potential and record current-time and charge-time data. The electrodeposition was performed for 17.5 min at a fixed cathodic potential E_V of -875 mV and a solution temperature of 80 ± 2 °C with moderate stirring.

2.3 Film characterization

Field-emission scanning electron microscopy (FESEM) was performed on a Hitachi S-4800 instrument to image the surface and cross-sectional morphologies of the electrodeposited ZnO films. The FESEM image, shown in figure 3(b), reveals a fully continuous ZnO film with large grain sizes and columnar crystalline structure. The ZnO film thickness is estimated to be 4700 ± 50 nm. X-ray diffraction (XRD) peak patterns were also collected with a Bruker D8 Discover diffractometer at a Cu-Kα line of 1.54059 Å. The XRD peak pattern displayed in figure 4 can be indexed to the Miller planes of hexagonal wurtzite ZnO (PDF card 01-089-1397). The narrowness of the diffraction peaks further attests to the large grain sizes in the ZnO thin film.

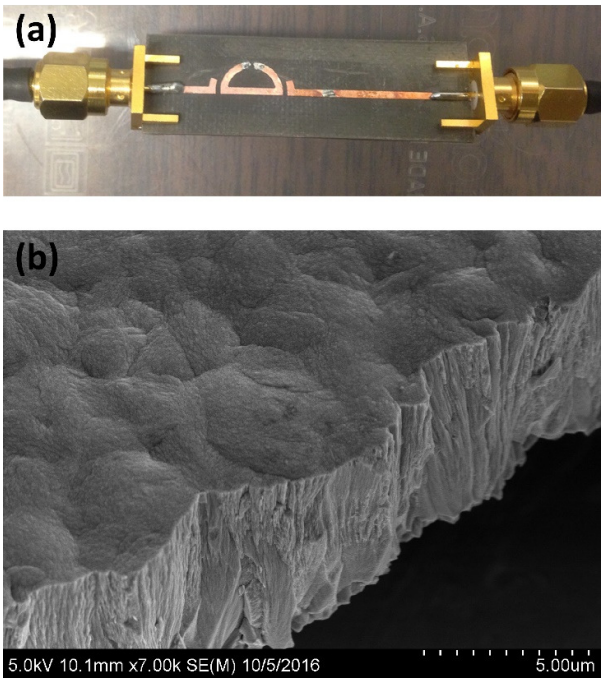

Figure 3. (a) The fabricated microwave resonator sensor, (b) FESEM images of the surface and cross-sectional morphologies of electrodeposited ZnO films on copper understructure.

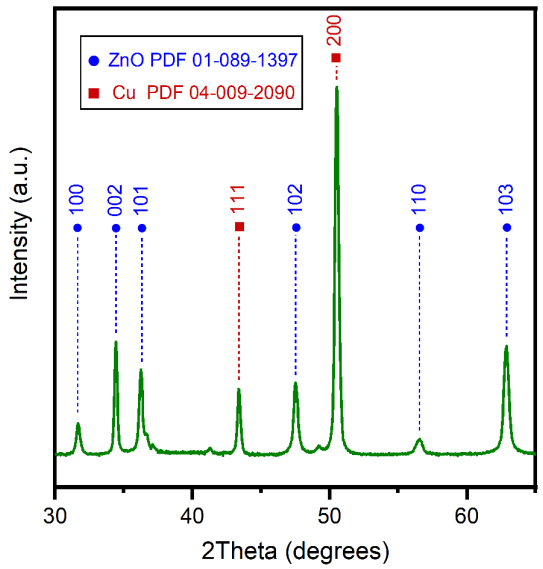

Figure 4. XRD peaks profile of the same electrodeposited ZnO film on copper understructure. The square symbol refers to the Cu material.

A thickness of 4700 ± 50 nm of ZnO thin film, as measured by cross-sectional FESEM, has been electrodeposited on the copper lines of the ring resonator. The backside copper metallization, forming the ground plane, was protected during the ZnO electrodeposition process. A UV curing lamp with 254 nm center-wavelength was utilized to illuminate the ZnO film during

the experiment. A PXI vector network analyzer (VNA) equipped with LabView software was used to automatically measure and record the S-parameters of the microwave structure. The data sampling was performed every 10 s over the frequency span of 6.15 to 6.35 GHz, with intermediate frequency bandwidth of 1 kHz and 2001 frequency sampling points, which will give us the frequency interval between samples of less than 100 KHz. Hence, the VNA parameters setting for all the experiments are kept within this range. Figure 5 shows the measurement setup for this test. The resonator with ZnO thin film was placed inside a dark-box to isolate and suppress the effect of the ambient light at room temperature (23 °C) with the relative humidity of 25%.

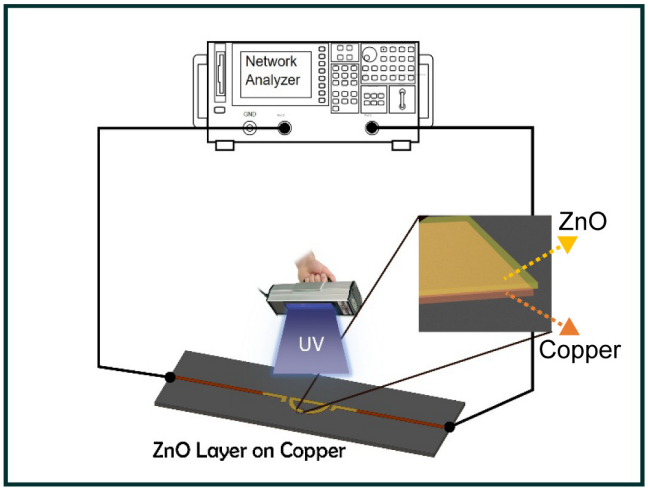

Figure 5. Schematic of the experimental setup. A UV lamp with wavelength of 254 nm was placed at a distance of 20 cm from the resonator.

Further studies were carried out to examine the effects of changing humidity levels on the photosensing reliability of the resonator sensor. To this effect, an experimental setup was prepared using dry air as the reference carrier gas, a bubbler as the source of humidity and two mass flow controllers (MFC) to dilute the humid air with dry air to create different humidity levels inside a sealed chamber. Figure 6 displays the experimental setup. A temperature/humidity sensor was placed inside the chamber along with the microwave sensor to monitor the relative humidity and the temperature as an independent reference.

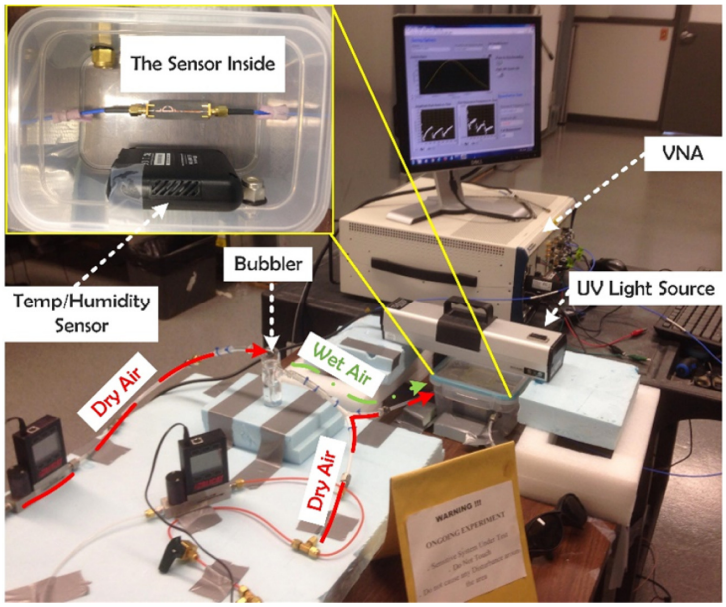

Figure 6. Experimental setup to study the effect of relative humidity on the response of the ZnO coating during the illumination and relaxation periods.

3. Results and Discussion

The experimental S_{21} parameters of the resonator, before and after the ZnO film electrodeposition, are presented in figure 7. It is observed that the resulting alteration of the effective permittivity of the microwve resonator causes downshift of the resonance frequency and decrease of the resonance amplitude. The respective quality factors computed from the data in fgure 7 are 119 and 118 for the bare and ZnO-coated resonators.

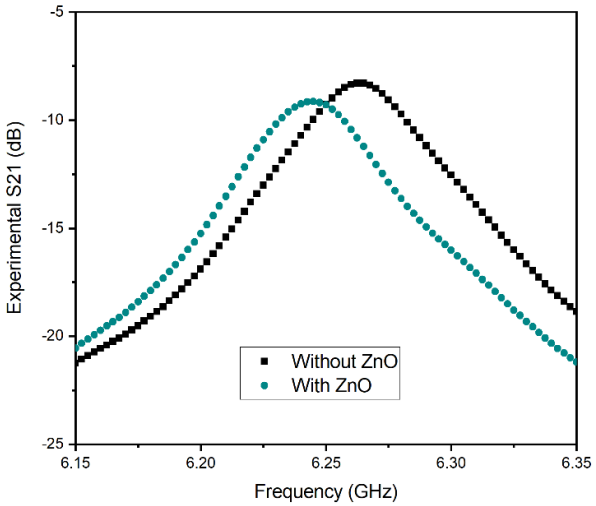

Figure 7. The experimental S_{21} parameters of the resonator, before and after the ZnO film electrodeposition, respectively.

The transient responses of the resonance frequency of the resonator sensor were extracted from the measured S_{21} resonance profile. Upon exposure to the UV illumination, the resonance frequency shifted downward and exhibited a significant downshift of ~ 6 MHz after an illumination time of 200 s. After the UV illumination is switched off, the profiles return back to their initial states after a time period of 900 s, as demonstrated by the transient responses in figure 8. The resonator sensor thus exhibits good sensitivity to UV light within a short exposure time of less than 3 min. While the transient photoresponses are fundamentally manifestations of band-to-band electron-hole pair generation-recombination upon UV light absorption, they are still strongly dependent on multiple other processes that could include: 1) trapping, detrapping, and recombination of photogenerated carriers by defect centers, 2) photoionization of oxygen vacancies [43], 3) adsorption and photodesorption of ambient oxygen and water on the surface and grain boundaries exposed to UV light, and 4) other processes. These processes contribute with varying weights to the observed relaxation to the initial state. It should be noted that the UV penetration depth in ZnO is less than 100 nm, whereas the thickness of our ZnO film is close to 5 μm. Therefore, only thin surface layers contribute to the UV photoresponse. The thickness of the ZnO film is still relevant because the density of grain boundaries and bulk defects within the UV-penetrated regions of the ZnO film depend on it [47].

We know that the electrical conductivity of the ZnO film rises when exposed to UV light. However, our microwave simulations have revealed that changes in tangent loss do not shift the resonance frequency of the microwave resonator in any consequential way. On the other hand, the simulations show that the resonance frequency downshifts when the dielectric constant $\varepsilon_r = \varepsilon'/\varepsilon_0$ of the coating film increases. An increase in the dielectric constant of the coating film would lead to an increase of the effective dielectric constant of the resonator system which, in turn, results in the observed downshift of the resonance frequency. Therefore, based on the simulation results, we conclude that the resonance frequency downshift, which has been measured experimentally, could result mainly from the changes of the dielectric constant of the ZnO film in response to UV illumination. Admittedly, photoexcitation and relaxation processes, some of which were listed earlier, are responsible for the changes of the dielectric constant. Indeed, they involve the creation of bound charges which alter the polarizability of

the ZnO material and hence its dielectric constant in accordance with the principle of the photodielectric effect [32]. In this respect, it should be emphasized again that the photoconductive effect has been predicted by simulations to not have a consequent influence on the resonance frequency shift of the transmitted microwave signal.

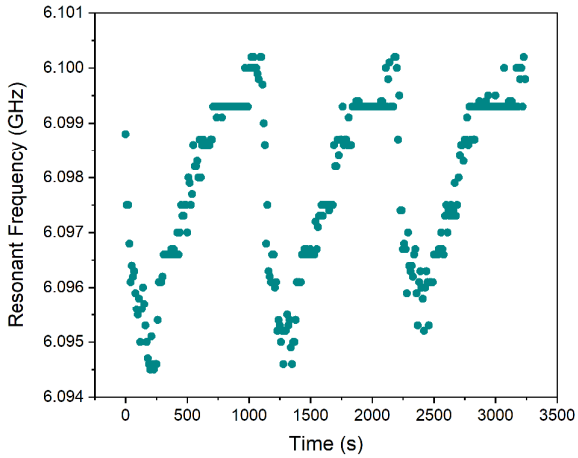

Figure 8. Resonance frequency variation with time for an illumination time of 200 s and a relaxation time of 900 s for three consecutive cycles.

It is of interest to study the excitation and relaxation curves of the transient photoresponse with their time constants at different humidity levels. Note that the relaxation time corresponds to the lifetime of photogenerated carriers. ZnO is widely recognized for its humidity sensing properties [48] and, therefore, our ZnO-based UV sensor performance is expected to depend on the ambient relative humidity (RH) levels.

The experimental setup for humidity study has been described in the Experimental section. The transient photoresponse of the resonance amplitude of the transmitted microwave signal was studied at different humidity levels. Figure 9(a) shows the measured results at 20% RH whereas figure 9(b) presents the same experiment with identical parameters at 70% RH. The UV-light was illuminated for 2 min (T_i) and the sample was relaxed for 6 min (T_r) for three consecutive cycles of UV light exposure/switch off.

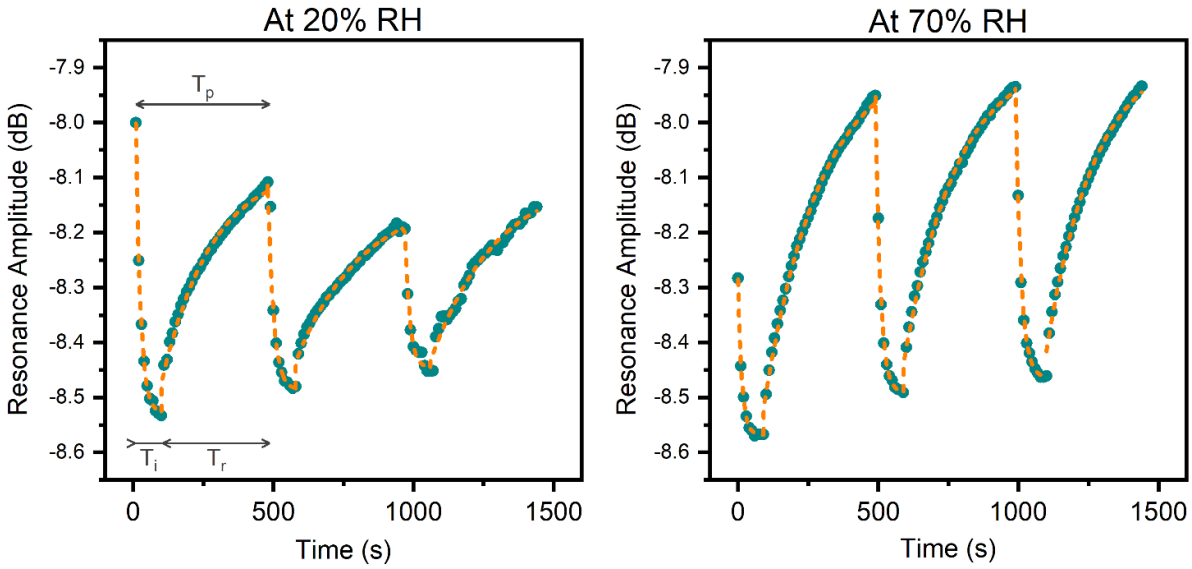

Figure 9. Resonance amplitude study during UV illumination and relaxation for three consecutive cycles at two RH levels: (a) RH = 20%, (b) RH = 70%. The curves could be fitted by a one-phase exponential decay function (dashed line).

During the 6 min relaxation times, the signal amplitude recoveries are much faster at 70% RH. As discussed earlier, the photoresponse processes at low RH include band-to-band electron-hole generation-recombination, defect-related traps and recombination centers, oxygen vacancies photoionization, and oxygen molecules adsorption/desorption on the surface and grain boundaries. Additionally, under the high RH condition, the role played by water vapor becomes important. The transient relaxation curves representing the total contributions from all these processes, displayed in figure 9, could be fitted by a one-phase exponential decay function with an average time constant τ_1 in the form of

$$A_r(t) = A_0 + A_1 e^{-(t-t_0)/\tau_1} \quad (2)$$

where t_0 is the time offset, A_0 the amplitude offset, and A_1 a fitting coefficient. The resonance amplitude fitting function parameters are summarized in table 2.

Table 2. First-order exponential function fitting parameters at different RH levels. For each RH level, a distinct time constant is given for each of the 3 cycles shown in figures 9(a) and 9(b). T_i and T_r refer to the illumination and relaxation time periods respectively. R-Square gives a statistical measure of the goodness of fit.

	Parameter(s)	RH = 20 %			RH = 70 %		
		1st cycle	2nd cycle	3rd cycle	1st cycle	2nd cycle	3rd cycle
T_r	Time Constant (τ_1)	177.0	231.8	232.9	199.2	186.2	171.2
	R-Square	0.9852	0.9813	0.9806	0.9960	0.9945	0.9944
T_i	Time Constant (τ_1)	16.2	20.3	16.4	13.2	17.1	18.9
	R-Square	0.9995	0.9995	0.9909	0.9978	0.9988	0.9979

From table 2, we derive that the average relaxation time constants are 213 s and 185 s at 20% RH and 70% RH respectively. The relaxation after exposure to UV light is thus faster at high RH. A major factor for this result is that oxygen molecules and water molecules adsorbed on the ZnO surface and grain boundaries interact differently with the photogenerated electrons and holes. At low RH, the predominance of adsorbed and ionized oxygen causes a large separation of the photogenerated holes from the photogenerated electrons. Such separation does not occur so extensively at high RH when the water molecules are predominant. Therefore, electrons and holes recombine much more quickly upon switching off the UV light, leading to a faster relaxation of the resonance amplitude [49].

The transient response of the resonance frequency and the quality factor of the measured profiles are presented in figure 10. According to the measured results, high RH leads to significant variations of the electrical parameters, extracted from the S_{21} resonance profile, of the ZnO-coated resonator sensor. The resonance frequency downshift during a short illumination time of 2 min reaches 3 MHz at 20% RH, whereas it is about 5 MHz at 70% RH. This increase of the resonance frequency downshift with RH could indicate that, due to the reactivity of water with both photogenerated electrons and holes [49], the effect of RH on the density of created bound charges is not negligible with respect to the effect of UV illumination [33]. To improve the sensor selectivity, it is thus preferable to implement a blocking action against the adsorption of water molecules on the surface and grain boundaries of the electrodeposited ZnO thin film.

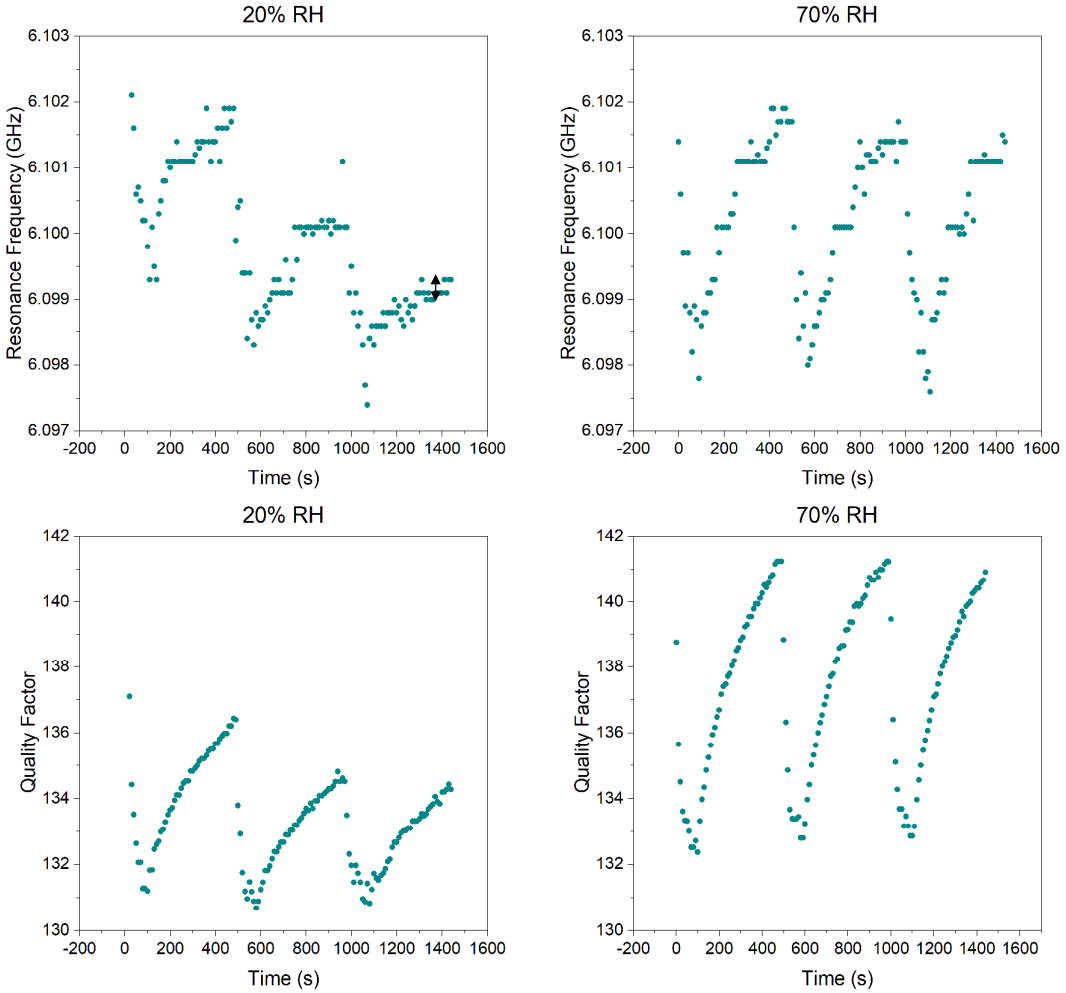

Figure 10. (a) Transient response of the resonance frequency at RH = 20%, (The arrow illustrates the sensor system readout precision)(b) transient response of the resonance frequency at RH = 70%, (c) quality factor variation at RH = 20%, and (d) quality factor variation at RH = 70%. For all experiments, the illumination time is 2 min and the relaxation time is 6 min.

In summary, we report the design, fabrication and characterization of a novel UV irradiation sensor. The device utilizes a simple and compact planar microwave resonator design that can be easily integrated on printed circuit boards. The insertion of the sensing ZnO thin film is achieved from an aqueous zinc nitrate solution by direct electrodeposition on the readily printed resonator circuit. A major attribute of this method is therefore the facile and low-cost fabrication as it does not involve any resource-intensive techniques such as photolithography or material deposition/removal in vacuum or environment-controlled systems. Time-resolved microwave measurements clearly demonstrated the sensitivity of the sensor at room temperature through downshifts of the resonance frequency and variations of the resonant signal amplitude and quality factor. The undesirable long-lived and persistent post-illumination effects, usually reported for ZnO thin films and nanostructures, were not observed in our sensor. The resonance frequency downshift could be mostly associated with the change in the ZnO film dielectric constant, and hence the effective dielectric constant of the multi-media resonator system. Such change would be brought about by additional bound charges, created by the trapping of photogenerated carriers, that are ultimately responsible for material polarizability alteration. In addition to this work, the impact of humidity on the microwave photoresponse has been studied experimentally. Induced carrier lifetimes were extracted at both low and high humidity levels and were found to be shorter with increased humidity. At high humidity levels, the sensor exhibits a larger resonance frequency downshift and faster relaxation. These effects derive from the different interaction mechanisms of the increased number density of adsorbed water molecules with the photogenerated carriers. These humidity effects are undesirable for the proper operation of the UV

irradiation sensor and should therefore be suppressed through the appropriate water blocking technique. Ultimately, the many advantages offered by the use of planar microwave electronics could be leveraged in the service of affordable and efficient microwave photosensing and sensing in general. In addition, such simplified time-resolved photoresponse methods offer considerable possibilities to conduct fundamental studies on charge carrier dynamics and material properties.

Acknowledgements

This research was supported by NSERC, CMC Microsystems, Future Energy Systems and Canada Research Chair program.

References

[1] Look D C 2001 Recent advances in ZnO materials and devices *Materials Science and Engineering B-Solid State Materials for Advanced Technology* **80** 383-387
[2] Mang A, Reimann K and Rubenacke S 1995 Band gaps, crystal-field splitting, spin-orbit coupling, and exciton binding energies in ZnO under hydrostatic pressure *Solid State Communications* **94** 251-254
[3] Thomas D G 1960 The exciton spectrum of zinc oxide *Journal of Physics and Chemistry of Solids* **15** 86-96
[4] Albrecht J D, Ruden P P, Limpijumnong S, Lambrecht W R L and Brennan K F 1999 High field electron transport properties of bulk ZnO *Journal of Applied Physics* **86** 6864-6867
[5] Soci C, Zhang A, Xiang B, Dayeh S A, Aplin D P R, Park J, Bao X Y, Lo Y H and Wang D 2007 ZnO Nanowire UV Photodetectors with High Internal Gain *Nano Letters* **7** 1003-1009
[6] Adl A H, Kar P, Farsinezhad S, Sharma H and Shankar K 2015 Effect of sol stabilizer on the structure and electronic properties of solution-processed ZnO thin films *RSC Advances* **5** 87007-87018
[7] Chen M T, Lu M P, Wu Y J, Song J H, Lee C Y, Lu M Y, Chang Y C, Chou L J, Wang Z L and Chen L J 2010 Near UV LEDs Made with in Situ Doped p-n Homojunction ZnO Nanowire Arrays *Nano Letters* **10** 4387-4393
[8] Lim J H, Kang C K, Kim K K, Park I K, Hwang D K and Park S J 2006 UV Electroluminescence Emission from ZnO Light-Emitting Diodes Grown by High-Temperature Radiofrequency Sputtering *Advanced Materials* **18** 2720-2724
[9] Renganathan B, Sastikumar D, Gobi G, Rajeswari Yogamalar N and Chandra Bose A 2011 Nanocrystalline ZnO coated fiber optic sensor for ammonia gas detection *Optics and Laser Technology* **43** 1398-1404
[10] Liu D and Kelly T L 2014 Perovskite solar cells with a planar heterojunction structure prepared using room-temperature solution processing techniques *Nat Photon* **8** 133-138
[11] Adl A H, Ma A, Gupta M, Benlamri M, Tsui Y Y, Barlage D W and Shankar K 2012 Schottky Barrier Thin Film Transistors Using Solution-Processed n-ZnO *ACS Applied Materials and Interfaces* **4** 1423-1428
[12] Ong B S, Li C, Li Y, Wu Y and Loutfy R 2007 Stable, Solution-Processed, High-Mobility ZnO Thin-Film Transistors *Journal of the American Chemical Society* **129** 2750-2751
[13] Chow T P and Tyagi R 1994 Wide bandgap compound semiconductors for superior high-voltage unipolar power devices *IEEE Transactions on Electron Devices* **41** 1481-1483
[14] Nause J E 1999 ZnO broadens the spectrum *III-Vs Review* **12** 28-31
[15] Moghadas H, Daneshmand M and Mousavi P 2011 A Dual-Band High-Gain Resonant Cavity Antenna With Orthogonal Polarizations *IEEE Antennas and Wireless Propagation Letters* **10** 1220-1223
[16] Moghadas H, Daneshmand M and Mousavi P 2013 Single-layer partially reflective surface for an orthogonally-polarised dual-band high-gain resonant cavity antenna *IET Microwaves Antennas and Propagation* **7** 656-662
[17] Verma A and Dube D C 2005 Measurement of dielectric parameters of small samples at X-band frequencies by cavity perturbation technique *IEEE Transactions on Instrumentation and Measurement* **54** 2120-2123
[18] Meriakri V V, Chigrai E E, Nikitin I P, Parkhomenko M P 2007 Dielectric properties of water solutions with small content of glucose in the millimeter-wave band and the determination of glucose in blood *Physics and Engineering of Microwaves, Millimeter and Submillimeter Waves and Workshop on Terahertz Technologies. MSMW'07. The Sixth Int. Kharkov Symp. on,* 873-877
[19] Baker-Jarvis J, Geyer R G, Grosvenor J H, Janezic M D, Jones C A, Riddle B, Weil C M and Krupka J 1998 Dielectric characterization of low-loss materials - A comparison of techniques *IEEE Transactions on Dielectrics and Electrical Insulation* **5** 571-577
[20] Milovanovic B, Ivkovic S and Tasic V 1998 A simple method for permittivity measuring using microwave resonant cavity *Proc. 12th Int. Conf. MIKON*, **3** 705-709
[21] Boybay M S and Ramahi O M 2012 Material Characterization Using Complementary Split-Ring Resonators *IEEE Transactions on Instrumentation and Measurement* **61** 3039-3046
[22] Zarifi M H, Shariaty P, Abdolrazzaghi M, Hashisho Z and Daneshmand M 2016 Particle size characterization using a high resolution planar resonator sensor in a lossy medium *Sensors and Actuators B-Chemical* **234** 332-337
[23] Alahnomi R A, Zakaria Z, Ruslan E and Bahar A A M 2016 A Novel Symmetrical Split Ring Resonator Based on Microstrip for Microwave Sensors *Measurement Science Review* **16** 21-27

[24] Zarifi M H, Farsinezhad S, Abdolrazzaghi M, Daneshmand M and Shankar K 2016 Selective microwave sensors exploiting the interaction of analytes with trap states in TiO2 nanotube arrays *Nanoscale* **8** 7466-7473
[25] Zarifi M H, Rahimi M, Daneshmand M and Thundat T 2016 Microwave ring resonator-based non-contact interface sensor for oil sands applications *Sensors and Actuators B-Chemical* **224** 632-639
[26] Zarifi M H, Sohrabi A, Shaibani P M, Daneshmand M and Thundat T 2015 Detection of Volatile Organic Compounds Using Microwave Sensors *IEEE Sensors Journal* **15** 248-254
[27] Khalifeh R, Lescop B, Gallee F and Rioual S 2016 Development of a radio frequency resonator for monitoring water diffusion in organic coatings *Sensors and Actuators A-Physical* **247** 30-36
[28] Bailly G, Harrabi A, Rossignol J, Stuerga D and Pribetich P 2016 Microwave gas sensing with a microstrip interDigital capacitor: Detection of NH3 with TiO2 nanoparticles *Sensors and Actuators B-Chemical* **236** 554-564
[29] Mason A, Korostynska O, Ortoneda-Pedrola M, Shaw A and Al-Shamma'a A 2013 A resonant co-planar sensor at microwave frequencies for biomedical applications *Sensors and Actuators A-Physical* **202** 170-175
[30] Korostynska O, Mason A and Al-Shamma'a A 2014 Microwave sensors for the non-invasive monitoring of industrial and medical applications *Sensor Review* **34** 182-191
[31] Fok M, Bashir M, Fraser H, Strouther N and Mason A 2015 A Novel Microwave Sensor to Detect Specific Biomarkers in Human Cerebrospinal Fluid and Their Relationship to Cellular Ischemia During Thoracoabdominal Aortic Aneurysm Repair *Journal of Medical Systems* **39**
[32] Zarifi M H, Mohammadpour A, Farsinezhad S, Wiltshire B D, Nosrati M, Askar A M, Daneshmand M and Shankar K 2015 Time-Resolved Microwave Photoconductivity (TRMC) Using Planar Microwave Resonators: Application to the Study of Long-Lived Charge Pairs in Photoexcited Titania Nanotube Arrays *The Journal of Physical Chemistry C* **119** 14358-14365
[33] Zarifi M H, Farsinezhad S, Wiltshire B D, Abdorrazaghi M, Mahdi N, Kar P, Daneshmand M and Shankar K 2016 Effect of phosphonate monolayer adsorbate on the microwave photoresponse of TiO2 nanotube membranes mounted on a planar double ring resonator *Nanotechnology* **27** 375201
[34] Kunst M and Beck G 1986 The study of charge carrier kinetics in semiconductors by microwave conductivity measurements *Journal of Applied Physics* **60** 3558-66
[35] Park J, Reid O G, Blackburn J L and Rumbles G 2015 Photoinduced spontaneous free-carrier generation in semiconducting single-walled carbon nanotubes *Nature Communications* **6**
[36] Kunst M, Abdallah O and Wunsch F 2002 Passivation of silicon by silicon nitride films *Solar Energy Materials and Solar Cells* **72** 335-41
[37] Liu K W, Ma J G, Zhang J Y, Lu Y M, Jiang D Y, Li B H, Zhao D X, Zhang Z Z, Yao B and Shen D Z 2007 Ultraviolet photoconductive detector with high visible rejection and fast photoresponse based on ZnO thin film *Solid-State Electronics* **51** 757-61
[38] Zhu Q, Xie C S, Li H Y and Zeng D W 2016 A method for modeling and deciphering the persistent photoconductance and long-term charge storage of ZnO nanorod arrays *Nano Research* **9** 2972-3002
[39] Benlamri M, Farsinezhad S, Barlage D W and Shankar K 2016 Low residual donor concentration and enhanced charge transport in low-cost electrodeposited ZnO *Journal of Materials Chemistry C* **4** 2279-2283
[40] Benlamri M, Farsinezhad S, Barlage D W and Shankar K 2016 Communication-High Performance Schottky Diodes on Flexible Substrates Using ZnO Electrodeposited on Cu *ECS Journal of Solid State Science and Technology* **5** P324-P326
[41] Benlamri M, Bothe K M, Ma A M, Shoute G, Afshar A, Sharma H, Mohammadpour A, Gupta M, Cadien K C, Tsui Y Y, Shankar K and Barlage D W 2014 High-mobility solution-processed zinc oxide thin films on silicon nitride *Physica Status Solidi-Rapid Research Letters* **8** 871-875
[42] Gurwitz R, Cohen R and Shalish I 2014 Interaction of light with the ZnO surface: Photon induced oxygen “breathing”, oxygen vacancies, persistent photoconductivity, and persistent photovoltage *Journal of Applied Physics* **115** 033701
[43] Zhu Q, Xie C, Li H and Zeng D 2016 A method for modeling and deciphering the persistent photoconductance and long-term charge storage of ZnO nanorod arrays *Nano Research* **9** 2972-3003
[44] Jeon S, Ahn S-E, Song I, Kim C J, Chung U I, Lee E, Yoo I, Nathan A, Lee S, Ghaffarzadeh K, Robertson J and Kim K 2012 Gated three-terminal device architecture to eliminate persistent photoconductivity in oxide semiconductor photosensor arrays *Nat Mater* **11** 301-305
[45] Ivanoff Reyes P, Ku C-J, Duan Z, Xu Y, Garfunkel E and Lu Y 2012 Reduction of persistent photoconductivity in ZnO thin film transistor-based UV photodetector *Applied Physics Letters* **101** 031118
[46] Ashkenov N, Mbenkum B N, Bundesmann C, Riede V, Lorenz M, Spemann D, Kaidashev E M, Kasic A, Schubert M, Grundmann M, Wagner G, Neumann H, Darakchieva V, Arwin H and Monemar B 2003 Infrared dielectric functions and phonon modes of high-quality ZnO films *Journal of Applied Physics* **93** 126-133
[47] Benlamri M, Wiltshire B D, Zhang Y, Mahdi N, Shankar K and Barlage D W 2019 High Breakdown Strength Schottky Diodes Made from Electrodeposited ZnO for Power Electronics Applications *ACS Applied Electronic Materials* **1** 13-17
[48] Kannan P K, Saraswathi R and Rayappan J B B 2010 A highly sensitive humidity sensor based on DC reactive magnetron sputtered zinc oxide thin film *Sensors and Actuators A-Physical* **164** 8-14
[49] Li Y B, Della Valle F, Simonnet M, Yamada I and Delaunay J J 2009 Competitive surface effects of oxygen and water on UV photoresponse of ZnO nanowires *Applied Physics Letters* **94** 023110